

# Separating water isotopologues using diffusion-regulatory porous materials

<https://doi.org/10.1038/s41586-022-05310-y>

Yan Su<sup>1</sup>, Ken-ichi Otake<sup>2</sup>, Jia-Jia Zheng<sup>3</sup>, Satoshi Horike<sup>2</sup>, Susumu Kitagawa<sup>2</sup>✉ & Cheng Gu<sup>1,4</sup>✉

Received: 3 March 2022

Accepted: 1 September 2022

Published online: 9 November 2022

 Check for updates

The discovery of a method to separate isotopologues, molecular entities that differ in only isotopic composition<sup>1</sup>, is fundamentally and technologically essential but remains challenging<sup>2,3</sup>. Water isotopologues, which are very important in biological processes, industry, medical care, etc. are among the most difficult isotopologue pairs to separate because of their very similar physicochemical properties and chemical exchange equilibrium. Herein, we report efficient separation of water isotopologues at room temperature by constructing two porous coordination polymers (PCPs, or metal–organic frameworks) in which flip-flop molecular motions within the frameworks provide diffusion-regulatory functionality. Guest traffic is regulated by the local motions of dynamic gates on contracted pore apertures, thereby amplifying the slight differences in the diffusion rates of water isotopologues. Significant temperature-responsive adsorption occurs on both PCPs: H<sub>2</sub>O vapour is preferentially adsorbed into the PCPs, with substantially increased uptake compared to that of D<sub>2</sub>O vapour, facilitating kinetics-based vapour separation of H<sub>2</sub>O/HDO/D<sub>2</sub>O ternary mixtures with high H<sub>2</sub>O separation factors of around 210 at room temperature.

To use isotopologues for important applications in science<sup>4,5</sup> and technology<sup>6,7</sup>, chemists attempt to separate isotopologues using simple strategies based on molecular chemistry, such as the bond dissociation of water isotopologues via electrolysis<sup>8</sup>, or the use of host materials, such as caged compounds<sup>9,10</sup> or rigid porous materials<sup>11,12</sup>, to capture one of the isotopologues. However, separating isotopologues has been difficult because of the inherently similar intramolecular structures and intermolecular interactions among isotopologues<sup>3,13</sup>. Water isotopologues are among the most difficult isotopologue pairs to separate (Extended Data Table 1)<sup>14,15</sup> because of their very similar physicochemical properties, such as freezing point (H<sub>2</sub>O 273.15 K versus D<sub>2</sub>O 276.94 K), boiling point (H<sub>2</sub>O 373.15 K versus D<sub>2</sub>O 374.56 K) and bond energy (H<sub>2</sub>O 458.9 kJ mol<sup>-1</sup> bond<sup>-1</sup> versus D<sub>2</sub>O 466.4 kJ mol<sup>-1</sup> bond<sup>-1</sup>) (Supplementary Table 1). These similarities lead to significant obstacles to separating H<sub>2</sub>O and D<sub>2</sub>O by traditional distillation and electrolysis methods. The chemical exchange equilibrium among H<sub>2</sub>O, HDO and D<sub>2</sub>O,  $K = [\text{HDO}(\text{liquid})]^2 / \{[\text{H}_2\text{O}(\text{liquid})] \times [\text{D}_2\text{O}(\text{liquid})]\} = 3.85$  at 298 K<sup>16</sup>, results in these three species always coexisting once H<sub>2</sub>O and D<sub>2</sub>O are mixed. Therefore, it is difficult to separate water isotopologues with methods such as the Geib–Spevack process, based on proton exchange at thermodynamical equilibrium. Additionally, the kinetic diameters of H<sub>2</sub>O and D<sub>2</sub>O are ultrasmall and precisely the same (2.64 Å), making adsorption-based separation using porous hosts considerably difficult. The separation of water isotopologues using porous material-based adsorbents has not been proposed so far, even though they have been developed for decades.

Herein, we provide unprecedented separation of water isotopologues without significant energy expenditure by a diffusion-regulatory mechanism. Water isotopologues do not show apparent diffusion-rate

differences even at low temperatures, whereas no porous host material that can regulate the diffusion of water isotopologues has been reported. The essence of our mechanism is to control the diffusion of water isotopologues and amplify their rate differences by using locally dynamic frameworks to induce the efficient separation of water isotopologues. The dynamic frameworks preferentially adsorb one isotopologue depending on the kinetic difference, even from water isotopologue mixtures, thus achieving efficient separation of water isotopologues in a kinetic vapour separation system.

Our strategy takes advantage of the dynamic nature of porous coordination polymers (PCPs) or metal–organic frameworks (MOFs), which provide framework flexibility to regulate guest traffic, as well as guest recognition for separation<sup>17–20</sup>. Specifically, PCPs were produced by encoding dynamic flip-flop molecular motions into a diffusion-regulatory gate functionality that features globally robust but locally flexible frameworks to regulate the diffusion of water isotopologues (Fig. 1), thereby exhibiting temperature-regulated sorption behaviour in which different diffusion rates distinguish the water isotopologues.

## PCP syntheses and structural analyses

The PCPs combining ultrasmall pores, dynamic gate functionality and water stability are crucial for recognizing water isotopologues. Rather than the softness of the global frameworks of PCPs, we have shown that the local dynamic properties of the components in the channel can distinguish between very similar molecular species by their different diffusion behaviours<sup>17</sup>. We call this the diffusion by local dynamic motion (DLDM) mechanism. To advance this mechanism, we encoded local-motion functionality to synthesize PCPs capable of

<sup>1</sup>State Key Laboratory of Luminescent Materials and Devices, Institute of Polymer Optoelectronic Materials and Devices, South China University of Technology, Guangzhou, P. R. China. <sup>2</sup>Institute for Integrated Cell-Material Sciences, Institute for Advanced Study, Kyoto University, Kyoto, Japan. <sup>3</sup>Laboratory of Theoretical and Computational Nanoscience, CAS Center for Excellence in Nanoscience, National Center for Nanoscience and Technology, Chinese Academy of Sciences, Beijing, P. R. China. <sup>4</sup>Guangdong Provincial Key Laboratory of Luminescence from Molecular Aggregates, South China University of Technology, Guangzhou, P. R. China. <sup>✉</sup>e-mail: kitagawa@icems.kyoto-u.ac.jp; gucheng@scut.edu.cn

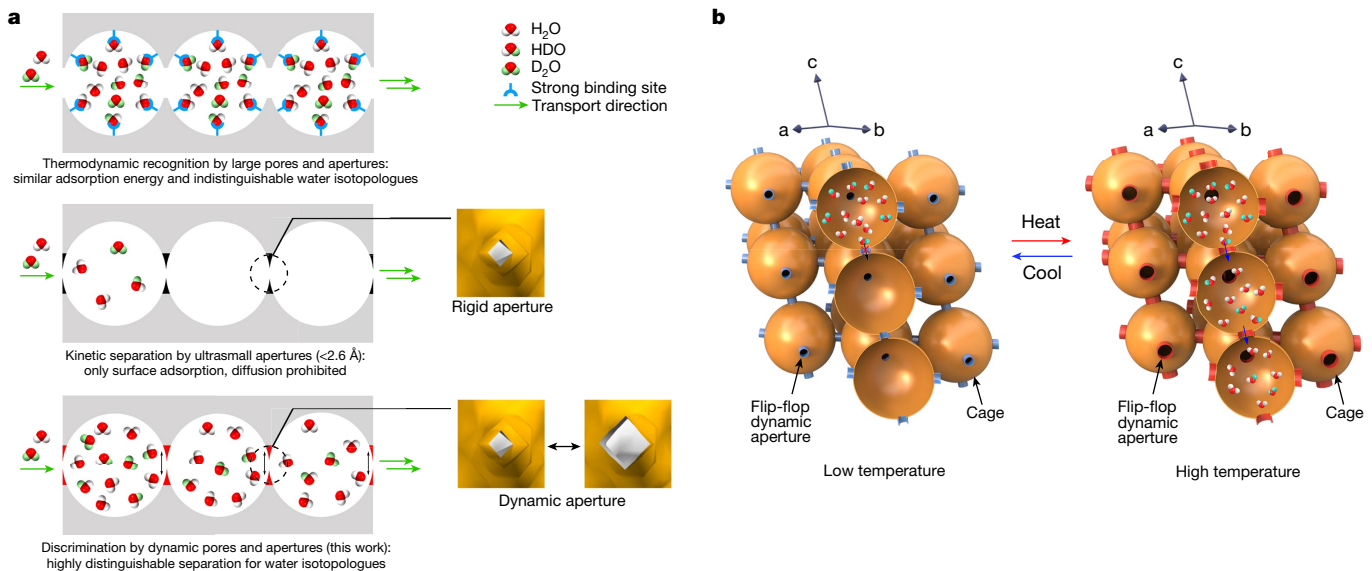


**Fig. 1 | The diffusion-regulatory mechanism for dynamic discrimination of water isotopologues.** **a**, Schematic representations of potential water-isotopologues discrimination mechanisms. Top: thermodynamic recognition by using strong binding sites; because of the very similar affinity of water isotopologues to the binding sites, to date, a successful example of this mechanism has not been demonstrated. Middle: kinetic separation by ultrasmall pores ( $<2.6\text{ \AA}$ ); because the apertures are rigid and are smaller than the kinetic diameters of water isotopologues, only surface adsorption can occur in this case. Bottom: kinetic discrimination by dynamic pores and apertures (this work); this mechanism involves a diffusion-regulatory pore system that can control the diffusion rates of water isotopologues, thereby

amplifying their diffusion-rate difference. **b**, Schematic diagram of the materials in this work which are designed by the diffusion-regulatory mechanism. Two PCPs with 3D transport pathways are constructed, which facilitate the efficient diffusion of water isotopologues. The apertures are coloured blue and red for the low- and high-temperature states, respectively. At low temperatures, the cage apertures are smaller than the kinetic diameters of the water isotopologues; hence, the cages are almost isolated, which impedes the adsorption of water isotopologues. With increasing temperature, the cage apertures become larger because of the thermal flipping of the gate moieties, and the cages open for water isotopologues adsorption at the given temperature.

recognizing water isotopologues. We call such PCPs flip-flop dynamic crystals (FDCs). To construct water-stable PCPs with much smaller pore apertures and locally dynamic functionality, we synthesized a Cu-based PCP with a dragonfly-type ligand comprising isophthalic acid and dibenzof[*b,f*]azepine (DBAP) moieties (DBAP-ipa; see Supplementary Material and Supplementary Figs. 1–13) with local motion; the adequate flipping energy of the latter moiety is less than  $20\text{ kJ mol}^{-1}$  (Supplementary Fig. 14). The as-synthesized PCP, namely, Cu(DBAP) (termed **FDC-1**) (Supplementary Figs. 15–18, Supplementary Tables 2 and 4 and Supplementary Data 1), possessed an NbO-type cage structure; one cage was surrounded by six open-metal sites on the Cu<sup>2+</sup> paddle wheels, four of which were occupied by *N,N*-dimethylacetamide (DMA) molecules (Supplementary Fig. 19) and the other two were coordinated with water molecules. Subsequently, **FDC-1** was subjected to vacuum at 393 K, resulting in its activated phase (**FDC-1a**, Supplementary Figs. 19–22 and Supplementary Table 4). **FDC-1a** maintained its robust three-dimensional (3D) structures upon activation (Fig. 2a). By contrast, the water molecules were excluded from the frameworks, and the DMA molecules remained fixed in the cages. The structure of **FDC-1a** features only one type of nanocage with six identical windows for the diffusion of water isotopologues (Fig. 2b). Each diffusion window contains a small triangular gate of only  $2.2\text{ \AA}$  in size, surrounded by two isophthalic units and two benzene rings of the DBAP moiety (Fig. 2c). To further demonstrate the diffusion-regulatory mechanism, we synthesized another ligand by replacing the DBAP moiety with the 2,2'-iminodibenzyl (IDB) moiety (IDB-ipa; see Supplementary Material and Supplementary Figs. 1–14). The corresponding Cu-based PCP, whether in the as-synthesized or activated phase (termed **FDC-2** and **FDC-2a**, respectively), adopts isostructures as **FDC-1** and **FDC-1a** (Fig. 2, Supplementary Figs. 15–22, Supplementary Tables 2–4 and Supplementary Data 2), whereas its diffusion window is  $2.0\text{ \AA}$  in size (Fig. 2d), slightly smaller than that of **FDC-1a**. The size of these cage

gates is expected to be temperature responsive due to thermal flipping of the DBAP or IDB unit, which facilitates the admission of water isotopologues at high temperatures (Fig. 1b) and blocks them at low temperatures. Therefore, the dynamic cage gates can amplify the difference in the diffusion rate of the water isotopologues. Moreover, the smaller apertures in **FDC-2a** are expected to show stricter diffusion regulation than **FDC-1a**, thereby better distinguishing water isotopologues.

### Vapour sorption

The H<sub>2</sub>O and D<sub>2</sub>O sorption curves for **FDC-1a** at 298 K exhibited similar profiles, with a gradual increase in the adsorption curve combined with an evident hysteresis during desorption (Fig. 3a). However, there was an apparent difference in the uptake amounts for H<sub>2</sub>O ( $36.1\text{ cm}^3\text{ g}^{-1}$ ) and D<sub>2</sub>O ( $25.9\text{ cm}^3\text{ g}^{-1}$ ) at a relative vapour pressure ( $P/P_s$ ) of 0.98. A similar trend was also observed in the case of **FDC-2a**; the uptake amounts at  $P/P_s$  of 0.98 for H<sub>2</sub>O and D<sub>2</sub>O were  $25.2$  and  $15.4\text{ cm}^3\text{ g}^{-1}$ , respectively (Fig. 3b). Accordingly, the uptake ratios of H<sub>2</sub>O/D<sub>2</sub>O were  $1.39$  and  $1.64$  for **FDC-1a** and **FDC-2a**, respectively, at 298 K and  $P/P_s$  of 0.98, thus indicating that the two PCPs selectively adsorb H<sub>2</sub>O over D<sub>2</sub>O. Notably, **FDC-1a** and **FDC-2a** preferentially adsorb H<sub>2</sub>O over D<sub>2</sub>O, and such a marked selectivity has not been observed for other small-pore adsorbents, including zeolites, activated carbons, and other PCPs/MOFs (Extended Data Fig. 1). Even though some compounds have slightly different adsorption preferences for water isotopologues, the difference in adsorption behaviour is not comparable to that of **FDC-1a** and **FDC-2a**.

Although the abovementioned sorption curves already revealed an apparent difference in the adsorption amounts of water isotopologues, they were not able to reflect the differences in the sorption kinetics. Therefore, we performed time-dependent adsorption of water isotopologues by **FDC-1a** and **FDC-2a**. Remarkable differences were observed

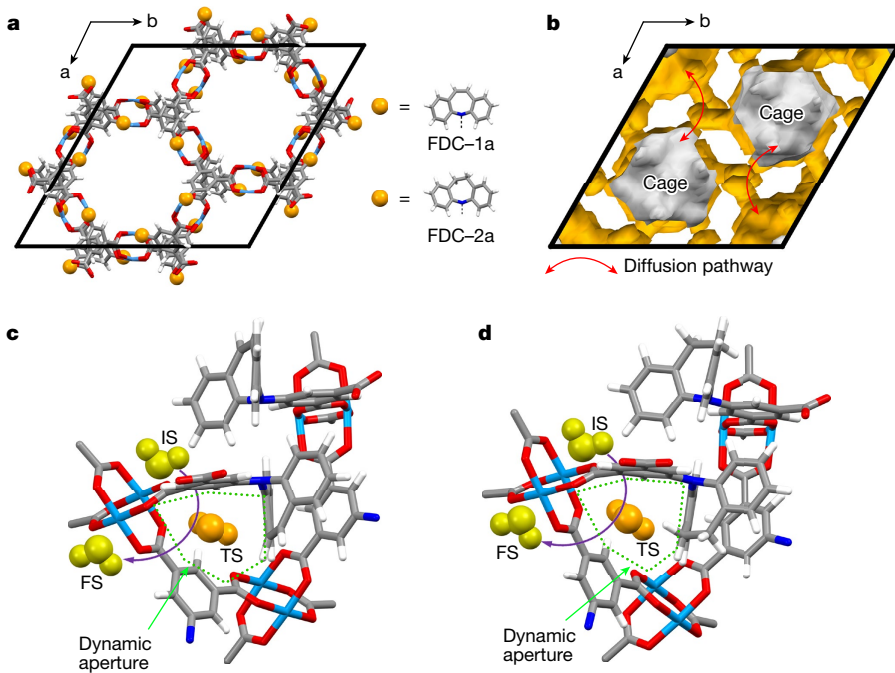


**Fig. 2 | Structural depictions of the diffusion-regulatory PCPs.** **a**, Crystal structures of **FDC-1a** and **FDC-2a** viewed along the *c* axis. The rhombus depicts the unit cell. C: grey; N: blue; O: red; Cu: sky blue. DMA molecules are omitted for clarity. **b**, View of the voids in **FDC-1a** and **FDC-2a** viewed along the *c* axis, where a small probe radius of 0.9 Å was used to visualize that the cage structure is interconnected with narrow windows. The void volumes are 2652 and 2722 Å<sup>3</sup> and correspond to 26.9% and 27.1% of the unit cell volumes for **FDC-1a** and

**FDC-2a**, respectively. The inner and outer surfaces of the cage are drawn in grey and orange, respectively. The red arrows indicate diffusion among cage windows, which are regulated by the dynamic aperture. **c**, Diffusion pathways and structures of the transition state in the activated phase of **FDC-1a**.

**d**, Diffusion pathways and structures of the transition state in the activated phase of **FDC-2a**. Water molecules in the initial state (IS)/final state (FS) and transition state (TS) are drawn in gold and orange, respectively.

in both **FDC-1a** and **FDC-2a**, and H<sub>2</sub>O diffused much faster than D<sub>2</sub>O (Fig. 3c,d). To obtain a similar uptake amount (for example, 30 cm<sup>3</sup> g<sup>-1</sup>), it takes at least 2.5-fold longer time for D<sub>2</sub>O compared to H<sub>2</sub>O. On the other hand, at the time of 2,100 s, the H<sub>2</sub>O adsorption amounts reached 30.3 and 26.3 cm<sup>3</sup> g<sup>-1</sup> for **FDC-1a** and **FDC-2a**, respectively, whereas the D<sub>2</sub>O adsorption amounts were only 9.1 and 5.1 cm<sup>3</sup> g<sup>-1</sup>. Accordingly, the uptake ratios of H<sub>2</sub>O/D<sub>2</sub>O were 3.3 and 5.2 for **FDC-1a** and **FDC-2a**. Such substantially high ratios were prerequisites for efficient dynamic separation of water isotopologues. Additionally, control experiments performed on the other small-pore absorbents revealed a negligible difference in the adsorption kinetics of water isotopologues (Supplementary Fig. 23).

## Adsorption kinetics

The kinetic factor is responsible for the preferential adsorption behaviour, as confirmed by further analyses (Supplementary Figs. 24–26) that excluded other possible factors, such as the thermal breathing effect<sup>21</sup>, crystallographic phase transitions<sup>22</sup> and instability upon sorption of water isotopologues<sup>23</sup>. The sorption behaviour clearly differed with increasingly prolonged exposure time (Extended Data Fig. 2). A jump increase at a low pressure of  $P/P_s < 0.2$  was observed for H<sub>2</sub>O and D<sub>2</sub>O in both PCPs. This change was attributed to the cluster formation of H<sub>2</sub>O or D<sub>2</sub>O in hydrophobic frameworks<sup>24</sup>, which was also confirmed by infrared spectra (Supplementary Fig. 27). The H<sub>2</sub>O or D<sub>2</sub>O uptake substantially increased to approximately 60 cm<sup>3</sup> g<sup>-1</sup> for **FDC-1a** and approximately 55 cm<sup>3</sup> g<sup>-1</sup> for **FDC-2a**. With prolonged exposure time, the system was more likely to reach a near-equilibrium state, as recognized by the reduced hysteresis in the desorption process; in this case, H<sub>2</sub>O and D<sub>2</sub>O could not be distinguished in **FDC-1a** and **FDC-2a** (Supplementary Fig. 28). These results demonstrated diffusion-regulated preferential adsorption that could only be achieved under kinetically

controlled non-equilibrium conditions<sup>17</sup>. Temperature-dependent sorption curves of H<sub>2</sub>O and D<sub>2</sub>O for **FDC-1a** and **FDC-2a** further confirmed the diffusion-regulatory features in the two PCPs. When the temperature was increased from 278 K to 323 K, the uptake of H<sub>2</sub>O substantially increased from 1.7 cm<sup>3</sup> g<sup>-1</sup> to 32.6 cm<sup>3</sup> g<sup>-1</sup> in **FDC-1a** and from 1.3 cm<sup>3</sup> g<sup>-1</sup> to 15.1 cm<sup>3</sup> g<sup>-1</sup> in **FDC-2a** ( $P/P_s = 0.3$ ), whereas the uptake of D<sub>2</sub>O apparently increased from 0.6 cm<sup>3</sup> g<sup>-1</sup> to 24.4 cm<sup>3</sup> g<sup>-1</sup> in **FDC-1a**, and from 0.5 cm<sup>3</sup> g<sup>-1</sup> to 11.8 cm<sup>3</sup> g<sup>-1</sup> in **FDC-2a** ( $P/P_s = 0.3$ ) (Extended Data Fig. 3). These uptake increases with increasing temperature can be viewed as a consequence of the diffusion limitation<sup>17,25</sup>. The diffusion process was characterized by the global  $P - D_s/R^2 - V$  and  $T - D_s/R^2 - V$  landscapes, with the diffusion rate quantified by Crank theory for every H<sub>2</sub>O or D<sub>2</sub>O adsorption plot in the 278–323 K range (Supplementary Materials), where  $V$  (millilitre per gram),  $P$  (kilopascal),  $T$  (Kelvin), and  $D_s/R^2$  (per second) denote the uptake volume, pressure, temperature, and diffusion rate, respectively, where  $R$  represents the radius of a PCP particle (Fig. 3e,f and Supplementary Figs. 29 and 30). These landscapes reveal that the small amounts of H<sub>2</sub>O or D<sub>2</sub>O adsorption at low temperatures are the result of their remarkably slow diffusion rates, which steadily increase with increasing temperature and pressure and thus lead to an increase in the adsorption amounts as the temperature rises to 323 K. The diffusion rate ( $D_s$ ) values of H<sub>2</sub>O in **FDC-1a** and **FDC-2a** were  $1.56 \times 10^{-2}$  and  $1.11 \times 10^{-2} R^2 s^{-1}$  at 298 K, which were 7.6- and 8.1-fold those of D<sub>2</sub>O ( $2.05 \times 10^{-3}$  and  $1.37 \times 10^{-3} R^2 s^{-1}$ , respectively). On the other hand, the diffusion rates of H<sub>2</sub>O and D<sub>2</sub>O in **FDC-1a** were 1.4- and 1.5-fold those in **FDC-2a** at 298 K, respectively, indicating faster diffusion kinetics in **FDC-1a**. **FDC-2a** possessed smaller cage apertures and lower diffusion rates than **FDC-1a**. Therefore, the adsorption amounts for H<sub>2</sub>O and D<sub>2</sub>O in **FDC-2a** were substantially lower than those in **FDC-1a**. These results indicate that diffusion of water isotopologues can be regulated by thermally controlling the size of cage gates of **FDC-1a** and **FDC-2a**, which consequently promotes effective vapour separation.

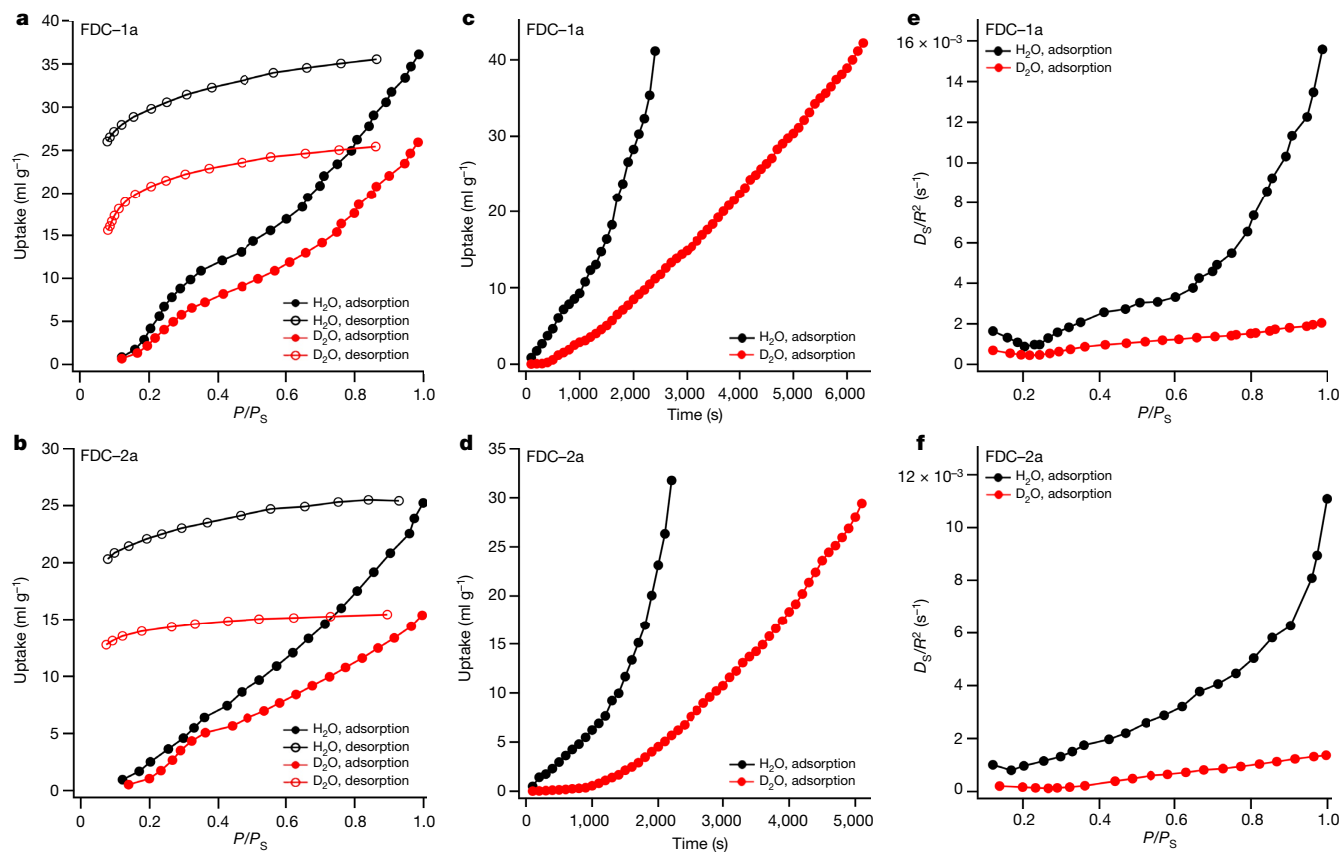


**Fig. 3 | Adsorption kinetics of water isotopologues for FDC-1a and FDC-2a.**

**a**, H<sub>2</sub>O and D<sub>2</sub>O sorption curves at 298 K for **FDC-1a**. The exposure time for each point is 600 s. **b**, H<sub>2</sub>O and D<sub>2</sub>O sorption curves at 298 K for **FDC-2a**. The exposure time for each point is 600 s. **c**, Time-dependent H<sub>2</sub>O and D<sub>2</sub>O

adsorption curves at 298 K for **FDC-1a**. The adsorption pressure is set to  $P/P_S = 1.0$ . **d**, Time-dependent H<sub>2</sub>O and D<sub>2</sub>O adsorption curves at 298 K for **FDC-2a**. The adsorption pressure is set to  $P/P_S = 1.0$ . **e**, Diffusion rates of H<sub>2</sub>O and D<sub>2</sub>O in **FDC-1a** at 298 K. **f**, Diffusion rates of H<sub>2</sub>O and D<sub>2</sub>O in **FDC-2a** at 298 K.

## VT-PXRD and computational studies

To understand the adsorption behaviour from a structural perspective, synchrotron powder X-ray diffraction (PXRD) patterns at various temperatures were collected, which revealed slight peak shifts to lower angles with increasing temperature under vacuum (Extended Data Fig. 4). Taking the peak corresponding to the (210) plane in **FDC-1a** as an example, the peak position shifted to the lower angle by 0.012° from 273 K to 373 K, consistent with the expansion of the [210] axis. Because the orientation of DBAP moieties is parallel to the (210) plane, such a small expansion can be caused by the thermal flipping of these moieties, which enlarges the cage gates (Supplementary Fig. 31). The same phenomena and related mechanisms were also present in **FDC-2a** (Supplementary Figs. 32 and 33). By contrast, no peak shift was observed when the synchrotron PXRD experiments were performed on water-adsorbed PCPs (Supplementary Figs. 34 and 35), suggesting a self-promoted adsorption process in which preabsorbed water isotopologue molecules kept the gate always open, facilitating subsequent adsorption.

Density functional theory calculations were carried out to understand the difference in the diffusion of water isotopologues in **FDC-1a** and **FDC-2a**. We noted that there is only one inter-cage diffusion pathway where one water molecule moves from one Cu site to another (Fig. 2c,d); for clarity, we considered that these two Cu sites were located in two different cages connected by a small aperture (Supplementary Figs. 17 and 18), although they belong to the same paddle-wheel unit. Experimental evidence obtained by means of synchrotron single-crystal XRD analysis of **FDC-1a** and **FDC-2a** sealed in H<sub>2</sub>O-filled capillaries allowed successful determination of the H<sub>2</sub>O location

(Supplementary Table 3 and Supplementary Data 3 and 4). The calculated barriers ( $\Delta E^\ddagger$ ) for H<sub>2</sub>O diffusion in **FDC-1a** and **FDC-2a** were 75.0 and 66.5 kJ mol<sup>-1</sup> (Supplementary Figs. 36 and 37, and Supplementary Tables 5 and 6), respectively, suggesting that it is difficult for H<sub>2</sub>O or D<sub>2</sub>O to freely enter or leave the pores of these two PCPs during adsorption. We further evaluated the activation energy ( $\Delta G^\ddagger$ ) for both H<sub>2</sub>O and D<sub>2</sub>O diffusions to elucidate the difference in their diffusion behaviour. The calculated  $\Delta G^\ddagger$  for D<sub>2</sub>O diffusion was slightly larger than that for H<sub>2</sub>O diffusion by 1.0 kJ mol<sup>-1</sup> and 2.1 kJ mol<sup>-1</sup> at 298 K in **FDC-1a** and **FDC-2a**, respectively (Supplementary Table 6). The smaller  $\Delta G^\ddagger$  for H<sub>2</sub>O diffusion indicates its faster diffusion rate in these two PCPs; indeed, the diffusion rate constant ( $k$ ) of H<sub>2</sub>O was almost double that of D<sub>2</sub>O, with  $k_{H_2O}/k_{D_2O}$  values of 1.5 and 2.3 at 298 K for **FDC-1a** and **FDC-2a**, respectively (Extended Data Fig. 5). Because the small apertures in **FDC-1a** and **FDC-2a** hinder H<sub>2</sub>O or D<sub>2</sub>O from freely entering their pores, the faster diffusion rate of H<sub>2</sub>O than that of D<sub>2</sub>O could enable more adsorption before reaching equilibrium, making it possible to kinetically recognize water isotopologues using **FDC-1a** and **FDC-2a**.

## Mixed vapour separation

Inspired by the sorption mechanism, we used **FDC-1a** and **FDC-2a** to carry out dynamic discrimination of vapour mixtures of water isotopologues with temperature-programmed desorption (TPD) protocol (Supplementary Fig. 38); these experiments were performed at 298 K with the vapour of an H<sub>2</sub>O/D<sub>2</sub>O mixture (H<sub>2</sub>O:D<sub>2</sub>O = 95:5, liquid volume). Once H<sub>2</sub>O and D<sub>2</sub>O are mixed, HDO is formed through chemical exchange equilibrium;  $K = [\text{HDO(liquid)}]^2 / \{[\text{H}_2\text{O(liquid)}] \cdot [\text{D}_2\text{O(liquid)}]\} = 3.85$  at

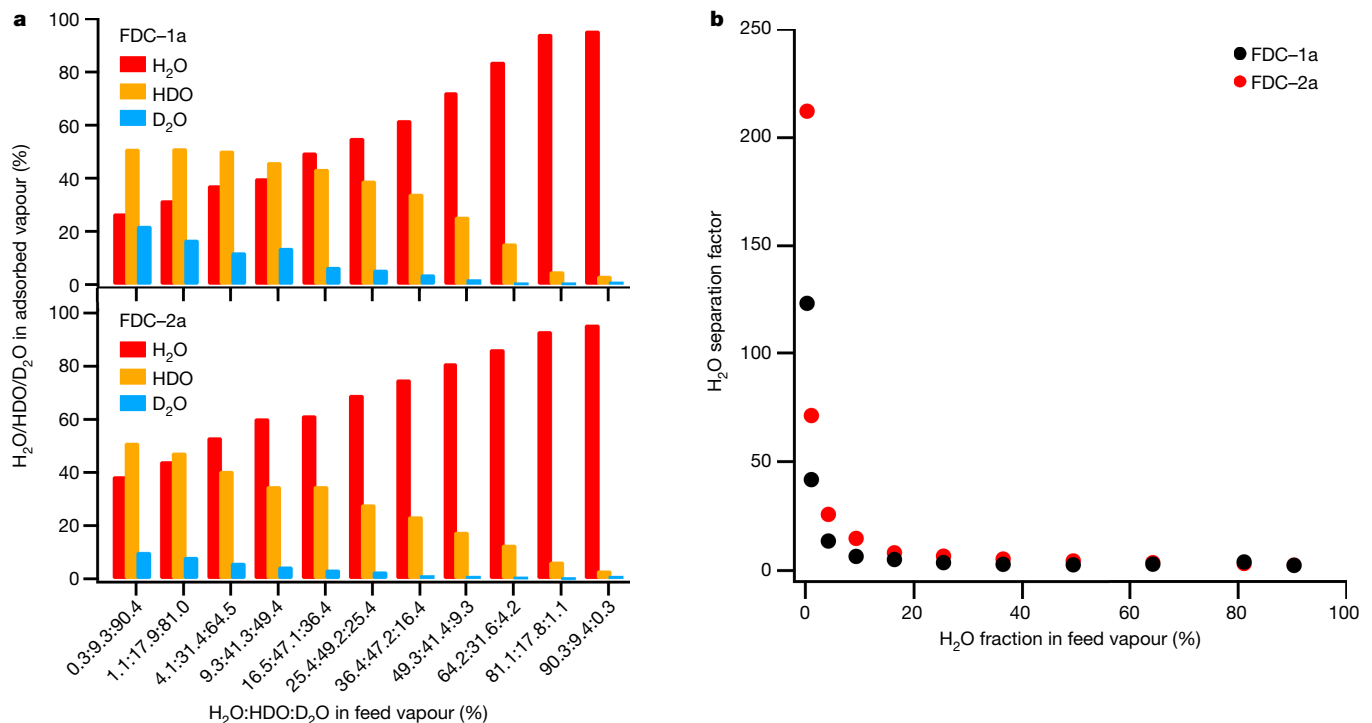


**Fig. 4 | Mixed vapour separation.** **a**, The correlation between water isotopologues in the feed vapour and the adsorbed vapour separated by **FDC-1a** and **FDC-2a** at 298 K. **b**, The correlation between H<sub>2</sub>O concentration in the feed vapour and the H<sub>2</sub>O separation factor for **FDC-1a** and **FDC-2a**.

298 K<sup>16</sup>. Therefore, we first measured the ratio of H<sub>2</sub>O, HDO and D<sub>2</sub>O in the vapour mixture by a mass detector before each separation experiment. For instance, in the case of H<sub>2</sub>O:D<sub>2</sub>O = 95:5 (liquid volume), the ratio was H<sub>2</sub>O:HDO:D<sub>2</sub>O = 90.3:9.4:0.3 in the feed vapour (Supplementary Fig. 39). Both **FDC-1a** and **FDC-2a** selectively adsorbed H<sub>2</sub>O from the H<sub>2</sub>O/HDO/D<sub>2</sub>O mixture within a short exposure time of 0.5 hours, leading to significant H<sub>2</sub>O enrichment, with compositions of 95.6% and 95.7% in the adsorbed phase (Fig. 4a and Supplementary Figs. 40 and 42) and H<sub>2</sub>O separation factors of 2.3 and 2.4 (Fig. 4b and Supplementary Figs. 41 and 43), respectively. The H<sub>2</sub>O separation factor decreased with prolonged exposure time (Supplementary Figs. 41 and 43), indicating that the separation performance is a result of faster H<sub>2</sub>O adsorption than that of HDO and D<sub>2</sub>O, causing H<sub>2</sub>O to occupy most of the available positions. Temperature-dependent separation experiments revealed that both **FDC-1a** and **FDC-2a** selectively adsorb H<sub>2</sub>O over a wide temperature range from 278 K to 323 K (Supplementary Figs. 44–47); the H<sub>2</sub>O separation factor in this temperature range did not obviously change, which was benefited by diffusion regulation of the water isotopologues within this temperature range. Remarkably, the separation performance of **FDC-1a** and **FDC-2a** was maintained over a wide range of feed-vapour compositions (Supplementary Figs. 48–77); for instance, even in a mixture with an extremely low H<sub>2</sub>O composition (H<sub>2</sub>O:HDO:D<sub>2</sub>O = 0.3:9.3:90.4), the H<sub>2</sub>O fractions in the adsorbed phases were enriched up to 26.8% and 38.6% by **FDC-1a** and **FDC-2a**, respectively (Fig. 4a and Supplementary Fig. 78), which corresponds to outstanding H<sub>2</sub>O separation factors of 123.5 and 212.1 (Fig. 4b). Compared with **FDC-1a**, **FDC-2a** exhibited substantial improvement in the H<sub>2</sub>O fraction in the adsorbed phase and the H<sub>2</sub>O separation factor at all feed-vapour compositions, which benefited from stricter diffusion regulation in **FDC-2a**, such that the slight difference in the diffusion rate of the water isotopologues was amplified. By contrast, other microporous materials, including zeolites, carbons and PCPs/MOFs with pore apertures from 2.1 Å to 3.0 Å, showed barely discrimination of water isotopologues (Supplementary Figs. 79–87), demonstrating that diffusion regulation is key to achieving water isotopologue

recognition. Static mixed-liquid co-adsorption experiments were carried out to demonstrate practical aspects of the separation capability of **FDC-1a** and **FDC-2a**. Selective H<sub>2</sub>O adsorption was observed by immersing **FDC-1a** and **FDC-2a** in an H<sub>2</sub>O:D<sub>2</sub>O = 7:3 (v/v, liquid volume) mixture (in which the ratio of H<sub>2</sub>O:HDO:D<sub>2</sub>O was 49.3:41.4:9.3) at 298 K for 7 days; the fraction of water isotopologues in the adsorbed phases and the H<sub>2</sub>O separation factors were 63.9:32.2:3.9 and 1.8 for **FDC-1a**, and 69.6:27.8:2.6 and 2.3 for **FDC-2a**, respectively (Supplementary Figs. 88 and 89).

## Outlook

This work demonstrates efficient distinguishing among water isotopologues at room temperature in two PCPs which amplifies their diffusion-rate difference. The TPD experiments demonstrate kinetics-based vapour separation of H<sub>2</sub>O/HDO/D<sub>2</sub>O ternary mixtures with high H<sub>2</sub>O separation factors of around 210 at 298 K. These outstanding discrimination features are attributed to the underlying mechanism, namely the DLDM mechanism, which was achieved by the co-operation of ultrasmall pore apertures and local dynamics of gate constituents. This rationale can be more broadly suitable for use with diverse adsorbents for the efficient discrimination of isotopologues.

## Online content

Any methods, additional references, Nature Research reporting summaries, source data, extended data, supplementary information, acknowledgements, peer review information; details of author contributions and competing interests; and statements of data and code availability are available at <https://doi.org/10.1038/s41586-022-05310-y>.

1. Muller, P. Glossary of terms used in physical organic chemistry. *Pure Appl. Chem.* **66**, 1077–1184 (1994).
2. Bigeleisen, J. Chemistry of isotopes. *Science* **147**, 463–471 (1965).
3. Kohen, A. & Limbach, H.-H. *Isotope Effects in Chemistry and Biology* (Wiley, 2005).

4. Levitt, M. H. *Spin Dynamics: Basics of Nuclear Magnetic Resonance* (John Wiley & Sons, 2001).
5. Huynh, M. H. V. & Meyer, T. J. Proton-coupled electron transfer. *Chem. Rev.* **107**, 5004–5064 (2007).
6. Sanderson, K. Big interest in heavy drugs. *Nature* **458**, 269–269 (2009).
7. Miller, A. I. & van Alstyne, H. M. Heavy Water: a Distinctive and Essential Component of CANDU. In *International Atomic Energy Agency technical committee meeting* (IAEA, 1993).
8. Lewis, G. N. & Macdonald, R. T. Concentration of H<sub>2</sub> isotope. *J. Chem. Phys.* **1**, 341–344 (1933).
9. Rechavi, D., Scarso, A. & Rebek, J. Isotopomer encapsulation in a cylindrical molecular capsule: a probe for understanding noncovalent isotope effects on a molecular level. *J. Am. Chem. Soc.* **126**, 7738–7739 (2004).
10. Mugridge, J. S., Bergman, R. G. & Raymond, K. N. Equilibrium isotope effects on noncovalent interactions in a supramolecular host-guest system. *J. Am. Chem. Soc.* **134**, 2057–2066 (2013).
11. Tanaka, H., Kanoh, H., Yudasaka, M., Lijiima, S. & Kaneko, K. Quantum effects on hydrogen isotope adsorption on single-wall carbon nanohorns. *J. Am. Chem. Soc.* **127**, 7511–7516 (2005).
12. Dunning, S. G. et al. A sensor for trace H<sub>2</sub>O detection in D<sub>2</sub>O. *Chem* **2**, 579–589 (2017).
13. Cai, J., Xing, Y. & Zhao, X. Quantum sieving: feasibility and challenges for the separation of hydrogen isotopes in nanoporous materials. *RSC Adv.* **2**, 8579–8586 (2012).
14. Liu, M. et al. Barely porous organic cages for hydrogen isotope separation. *Science* **366**, 613–620 (2019).
15. Kim, J. Y., Oh, H. & Moon, H. R. Hydrogen isotope separation in confined nanospaces: carbons, zeolites, metal-organic frameworks, and covalent organic frameworks. *Adv. Mater.* **31**, 1805293 (2019).
16. Bigeleisen, J., Lee, M. W. & Mandel, F. Equilibrium isotope effects. *Annu. Rev. Phys. Chem.* **24**, 407–440 (1973).
17. Gu, C. et al. Design and control of gas diffusion process in a nanoporous soft crystal. *Science* **363**, 387–391 (2019).
18. Banerjee, D., Simon, C. M., Elsaidi, S. K., Haranczyk, M. & Thallapally, P. K. Xenon gas separation and storage using metal-organic frameworks. *Chem* **4**, 466–494 (2018).
19. Jiang, H., Alezi, D. & Eddaoudi, M. A reticular chemistry guide for the design of periodic solids. *Nat. Rev. Mater.* **6**, 466–487 (2021).
20. Katsoulidis, A. P. et al. Chemical control of structure and guest uptake by a conformationally mobile porous material. *Nature* **565**, 213–217 (2019).
21. Henke, S., Schneemann, A. & Fischer, R. A. Massive anisotropic thermal expansion and thermo-responsive breathing in metal-organic frameworks modulated by linker functionalization. *Adv. Funct. Mater.* **23**, 5990–5996 (2013).
22. Salles, F. et al. Molecular dynamics simulations of breathing MOFs: structural transformations of MIL-53(Cr) upon thermal activation and CO<sub>2</sub> adsorption. *Angew. Chem. Int. Ed.* **47**, 8487–8491 (2008).
23. Kaye, S. S., Dailly, A., Yaghi, O. M. & Long, J. R. Impact of preparation and handling on the hydrogen storage properties of Zn<sub>4</sub>O(1,4-benzenedicarboxylate)<sub>3</sub> (MOF-5). *J. Am. Chem. Soc.* **129**, 14176–14177 (2007).
24. Furukawa, H. et al. Water adsorption in porous metal-organic frameworks and related materials. *J. Am. Chem. Soc.* **136**, 4369–4381 (2014).
25. Li, G. K. et al. Temperature-regulated guest admission and release in microporous materials. *Nat. Commun.* **8**, 15777 (2017).

**Publisher's note** Springer Nature remains neutral with regard to jurisdictional claims in published maps and institutional affiliations.

Springer Nature or its licensor holds exclusive rights to this article under a publishing agreement with the author(s) or other rightsholder(s); author self-archiving of the accepted manuscript version of this article is solely governed by the terms of such publishing agreement and applicable law.

© The Author(s), under exclusive licence to Springer Nature Limited 2022

## Methods

### Synthesis of FDC-1 and FDC-2

First, 500 mg (1.40 mmol) **DBAP-ipa** was dissolved in 50 ml DMA at room temperature. An aqueous solution (50 ml) of Cu(NO<sub>3</sub>)<sub>2</sub>·3H<sub>2</sub>O (676 mg, 2.80 mmol) was added to the above solution. Then the mixture was heated at 80 °C for 24 hours. The Cu(DBAP) was obtained as black-green block crystals with sizes up to several millimetres (538 mg, yield = 78%). The crystals were filtered, washed with DMA (50 ml three times) and water (50 ml, three times), and dried in air. The Cu(IDB) single crystals could be obtained by using the same method with a yield of 80%. The as-synthesized **FDC-1** and **FDC-2** were characterized by infrared spectra (Supplementary Fig. 16). The adsorption peak of the stretching vibration of the C=O double bond shifted to a low wave-number, indicative of the coordination bond formation in the PCPs.

### Solvent exchange and activation of FDC-1 and FDC-2

To measure the vapour adsorption property of **FDC-1** and **FDC-2**, we exchanged the guest and coordination solvents (DMA and water) with methanol by soaking **FDC-1** and **FDC-2** into methanol at 60 °C for 7 days. Every 8 hours, the methanol was replaced by a new one. After the exchange, the PCPs were dried under vacuum at 60 °C for 3 hours. <sup>1</sup>H NMR confirmed that the DMA and H<sub>2</sub>O in the PCPs cannot be exchanged by methanol (Supplementary Fig. 19). Therefore, we directly evacuated the PCPs at 393 K to remove the H<sub>2</sub>O molecules and produce activated phases.

The TG curve showed that the frameworks of the exchanged **FDC-1** and **FDC-2** were thermally stable until 282 °C and 271 °C, respectively, whereas at 120 °C the PCP lost the water molecules (Supplementary Fig. 20). Thus, we activated the PCPs at 120 °C for 11 hours to afford **FDC-1a** and **FDC-2a**; this temperature ensured complete removal of the water solvents, meanwhile excluding the possibility of framework decomposition.

### Vapour sorption measurements

Vapour sorption measurements were performed on BELSORP-max (MicrotracBEL, Japan, Corp.) automated volumetric sorption analyzers. A temperature-controlled water-bath system was equipped to regulate the sorption temperature. The powder sample of **FDC-1a** and **FDC-2a** (0.10 g) was placed in the sample cells and activated at 393 K under vacuum for 10 hours. The sample cells were then placed on BELSORP-max for vapour sorption measurements.

### Vapour separation experiments by temperature-programmed desorption (TPD) protocol

The TPD experiments on **FDC-1a** and **FDC-2a** were carried out as the following steps using BEL-CAT II cooperated with a mass detector (MicrotracBEL, Japan, Corp.). All experimental steps were performed at atmospheric pressure. The steps below were carried out similar to steps reported previously<sup>15,26</sup>.

#### (1) Measuring the feed-vapour components:

The temperature was controlled to 298 K, then He flow was bubbled to a liquid mixture of H<sub>2</sub>O and D<sub>2</sub>O, and the mixed vapour (volume ratios controlled by mass-flow controllers, the total flow rate at 10 sccm) flowed at ambient pressure. The vapour was examined with a mass detector and the ratios among H<sub>2</sub>O, HDO, and D<sub>2</sub>O were evaluated from the mass signal. The amounts of H<sub>2</sub>O, HDO and D<sub>2</sub>O in the feed vapour were calculated by integrating the area of the mass signal after the baseline subtraction.

#### (2) Sample loading and activation:

The powder sample of **FDC-1a** and **FDC-2a** (0.40 g) was filled in the cylindrical cell (8 mmφ) and activated at 393 K under vacuum for 10 hours. The sample cell was then placed on BEL-CAT II. The sample was then in-situ activated by flowing He at a constant rate of 10 sccm for 1 hour at 393 K. The twice activation ensured the complete removal of water adsorbed in the PCPs.

### (3) Adsorption process:

The temperature was decreased from 393 to 298 (or 278, 288, 308 and 323) K at a rate of 10 K min<sup>-1</sup>. Once the temperature reached 298 K, the He flow bubbled to a liquid mixture of H<sub>2</sub>O and D<sub>2</sub>O, and then the mixed vapour (volume ratios controlled by mass-flow controllers, the total flow rate at 10 sccm) flowed at ambient pressure, and the temperature was kept at 298 (or 278, 288, 308 and 323) K for a certain period under flowing mixed vapour.

### (4) Flowing away the non-adsorbed vapour:

The bubbling was stopped, and the remaining vapour in the cell and gas lines was flowed away by He with a flow rate of 10 sccm for 1 hour at 298 (or 278, 288, 308 and 323) K.

### (5) Release and detection of the adsorbed vapour:

After flowing away the non-adsorbed vapour, the temperature of the sample cell was increased to 393 K at a rate of 10 K min<sup>-1</sup> for releasing the adsorbed vapour, while the He flow was kept at a 10 sccm flow rate to carry the vapour to the detector. The released vapour was examined with a mass detector, and the ratios among H<sub>2</sub>O, HDO and D<sub>2</sub>O were evaluated from the mass signal. The amounts of released H<sub>2</sub>O, HDO and D<sub>2</sub>O were calculated by integrating the area of the mass signal after the baseline subtraction. The H<sub>2</sub>O separation factor  $\alpha$  is defined as:

$$\alpha = \frac{X_{\text{H}_2\text{O}}/Y_{\text{H}_2\text{O}}}{(X_{\text{HDO}}+X_{\text{D}_2\text{O}})/(Y_{\text{HDO}}+Y_{\text{D}_2\text{O}})} = \frac{X_{\text{H}_2\text{O}}/(X_{\text{HDO}}+X_{\text{D}_2\text{O}})}{Y_{\text{H}_2\text{O}}/(Y_{\text{HDO}}+Y_{\text{D}_2\text{O}})}$$

where  $X_{\text{H}_2\text{O}}$  is the concentration of H<sub>2</sub>O in the adsorbed phase,  $Y_{\text{H}_2\text{O}}$  is the concentration of H<sub>2</sub>O in the feed vapour,  $X_{\text{HDO}}$  is the concentration of HDO in the adsorbed phase,  $Y_{\text{HDO}}$  is the concentration of HDO in the feed vapour,  $X_{\text{D}_2\text{O}}$  is the concentration of D<sub>2</sub>O in the adsorbed phase and  $Y_{\text{D}_2\text{O}}$  is the concentration of D<sub>2</sub>O in the feed vapour.

## Data availability

The data that support the plots within this paper and other findings of this study are available from the corresponding authors upon request. The X-ray crystallographic coordinates for structures reported in this Article have been deposited at the Cambridge Crystallographic Data Centre (CCDC), under deposition numbers CCDC 2100317–2100320. These data can be obtained free of charge from the Cambridge Crystallographic Data Centre via [https://www.ccdc.cam.ac.uk/data\\_request/cif](https://www.ccdc.cam.ac.uk/data_request/cif).

26. Scott, H. S. et al. Highly selective separation of C<sub>2</sub>H<sub>2</sub> from CO<sub>2</sub> by a new dichromate-based hybrid ultramicroporous material. *ACS Appl. Mater. Interfaces* **9**, 33395–33400 (2017).
27. Oh, H., Park, K. S., Kalidindi, S. B., Fischer, R. A. & Hirscher, M. Quantum cryo-sieving for hydrogen isotope separation in microporous frameworks: an experimental study on the correlation between effective quantum sieving and pore size. *J. Mater. Chem. A* **1**, 3244–3248 (2013).
28. Zhang, L. et al. Exploiting dynamic opening of apertures in a partially fluorinated MOF for enhancing H<sub>2</sub> desorption temperature and isotope separation. *J. Am. Chem. Soc.* **141**, 19850–19858 (2019).
29. Zhao, X. et al. Hysteretic adsorption and desorption of hydrogen by nanoporous metal-organic frameworks. *Science* **306**, 1012–1015 (2004).
30. Chui, S. S.-Y., Lo, S. M.-F., Charmant, J. P. H., Orpen, A. G. & Williams, I. D. A chemically functionalizable nanoporous material [Cu<sub>3</sub>(TMA)<sub>2</sub>(H<sub>2</sub>O)<sub>3</sub>]<sub>n</sub>. *Science* **283**, 1148–1150 (1999).

**Acknowledgements** This work was supported by the National Natural Science Foundation of China (grant no. 21975078), the Guangdong Basic and Applied Basic Research Foundation (grant no. 2021A1515010311), the Natural Science Foundation of Guangdong Province (grant no. 2019B030301003), the 111 Project (grant no. BP0618009), the Thousand Youth Talents Plan, the KAKENHI Grant-in-Aid for Scientific Research (S) (grant nos. JP18H05262/JP22H05005) from the Japan Society of the Promotion of Science (JSPS). The synchrotron radiation experiments were performed at BLO2B1 and BLO2B2 of Spring-8 with the Japan Synchrotron Radiation Research Institute (JASRI) (Proposal nos. 2020A0649, 2020A1469, 2020A0617, and 2021A1104). We thank S. Kawaguchi and Y. Kubota for their help with VT-XRD measurements at Spring-8, the iCeMS analysis centre for access to the analytical instruments, and S. Sakaki at Kyoto University for access to VASP and computer resources. Y.S. acknowledges the scholarship support from the China Scholarship Council (grant no. 202006150059).

# Article

**Author contributions** Y.S. performed experiments associated with molecular synthesis, crystal growth, vapour sorption and vapour separation. K.O. and Y.S. conducted single-crystal and powder X-ray diffraction studies and structure analyses. J.-J.Z. carried out calculation studies. S.H. performed NMR analysis. C.G. and S.K. conceived the project and directed the research. All authors contributed to the writing and editing of the manuscript.

**Competing interests** The authors declare no competing interests.

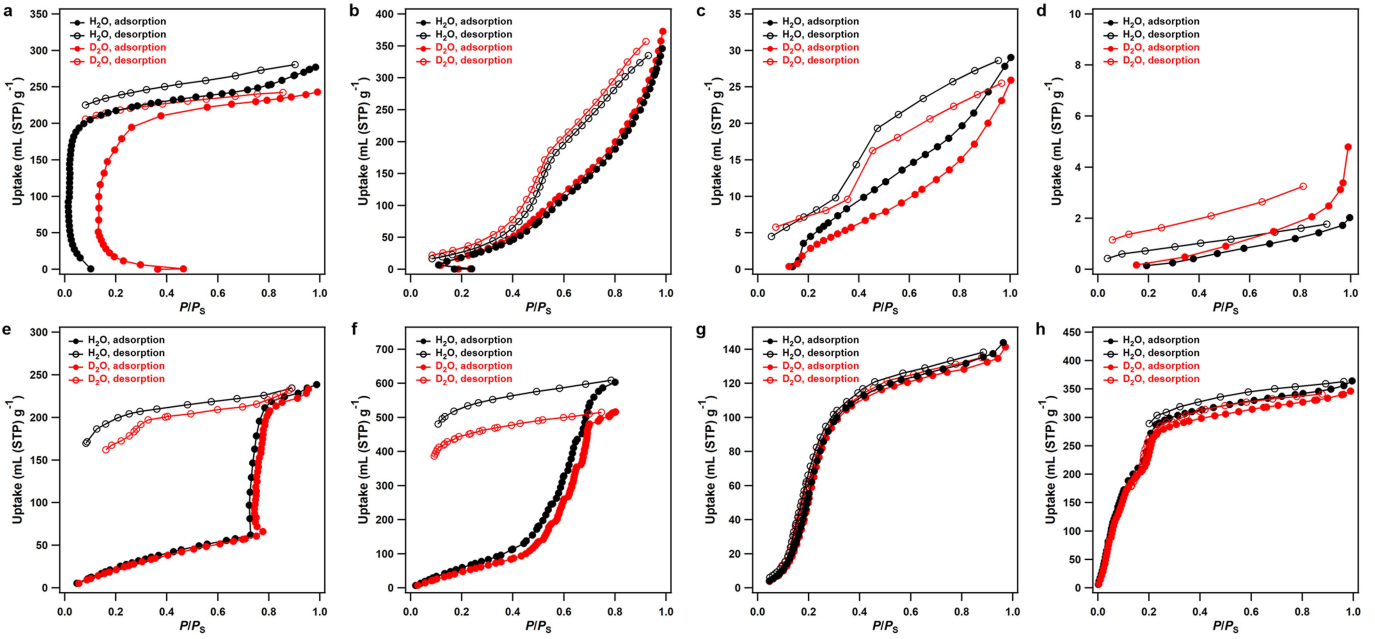
## Additional information

**Supplementary information** The online version contains supplementary material available at <https://doi.org/10.1038/s41586-022-05310-y>.

**Correspondence and requests for materials** should be addressed to Susumu Kitagawa or Cheng Gu.

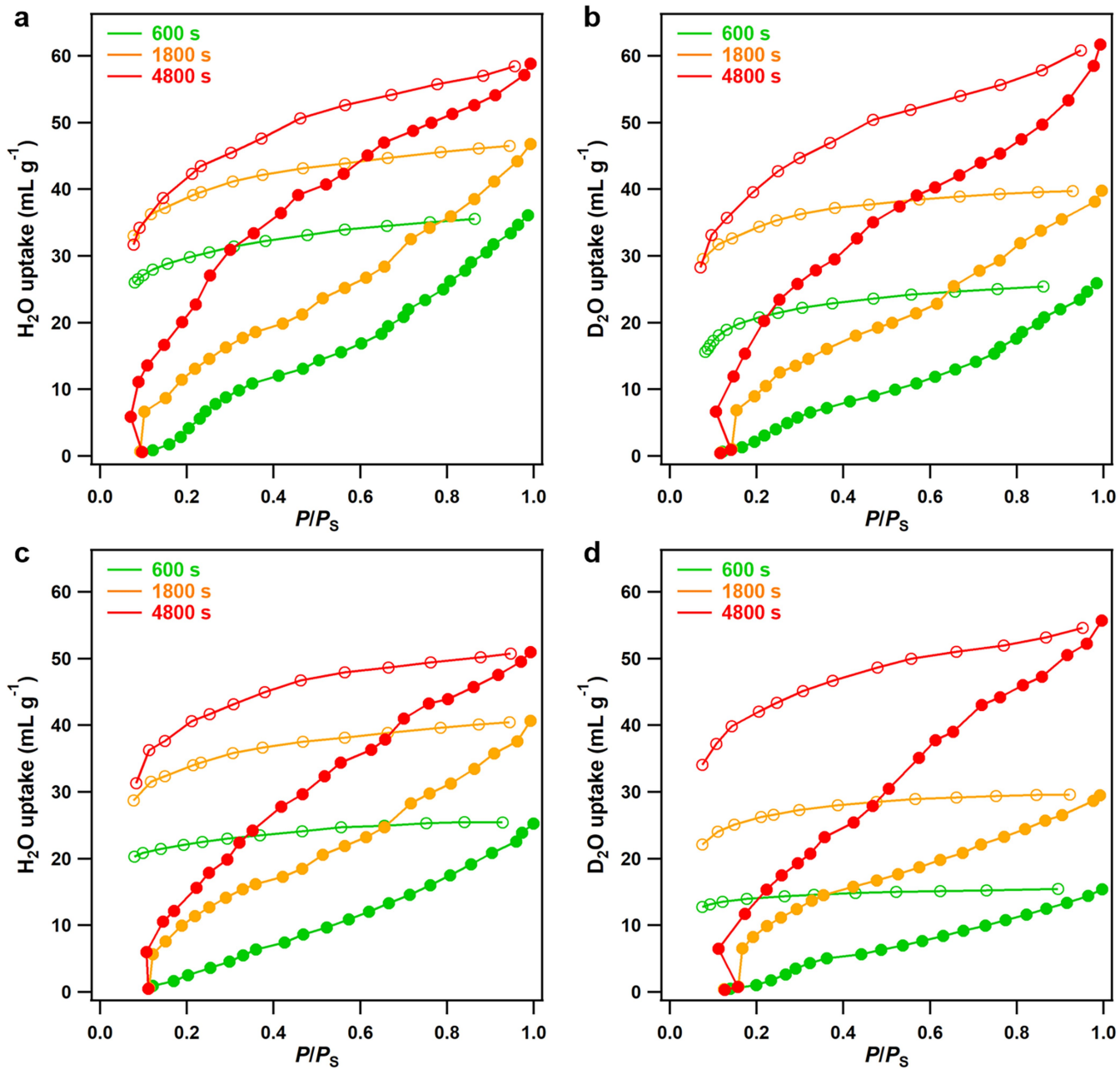
**Peer review information** *Nature* thanks Randall Snurr, Vincent Guillerm and the other, anonymous, reviewer(s) for their contribution to the peer review of this work.

**Reprints and permissions information** is available at <http://www.nature.com/reprints>.



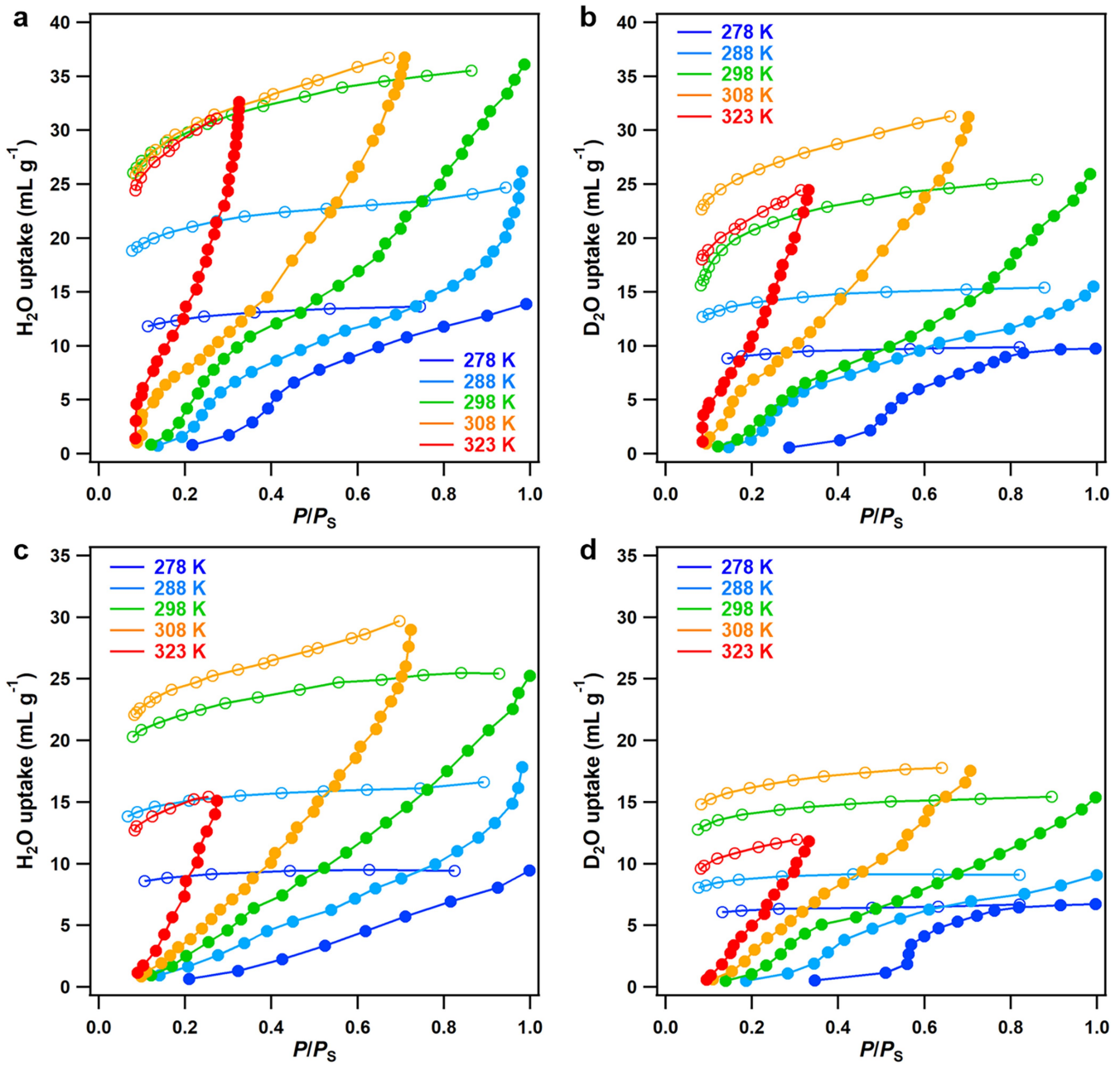
**Extended Data Fig. 1 | Vapour sorption for control materials.**  $\text{H}_2\text{O}$  and  $\text{D}_2\text{O}$  sorption curves at 298 K for (a) zeolite 3A (pore aperture 3 Å), (b) microporous active carbon (pore aperture 3 Å), (c) ZIF-7 (pore aperture 3 Å)<sup>27</sup>, (d) FMOF-Cu (pore aperture 2.5 Å)<sup>28</sup>, (e)  $\text{Ni}_2(\text{bipy})_3(\text{NO}_3)_4\text{-M}$  (pore aperture 2.4 Å)<sup>29</sup>, (f)  $\text{Ni}_2(\text{bipy})_3(\text{NO}_3)_4\text{-E}$  (pore aperture 2.1 Å)<sup>29</sup>, (g) Cu(OPTz) (pore aperture 3 Å)<sup>21</sup>, and (h) HKUST-1 (pore aperture 9 Å)<sup>30</sup>. For microporous active carbon and Cu(OPTz), their curves for  $\text{H}_2\text{O}$  and  $\text{D}_2\text{O}$  sorption were the same, and no discrimination was observed. For FMOF-Cu, the adsorption amounts for  $\text{H}_2\text{O}$  and  $\text{D}_2\text{O}$  were too low for adsorption-based separation. For ZIF-7, the difference in adsorption amounts for  $\text{H}_2\text{O}$  and  $\text{D}_2\text{O}$  were only 4.1 and  $3.1 \text{ cm}^3 \text{ g}^{-1}$  at  $P/P_s = 0.5$  and 0.98, respectively, not as large as in **FDC-1a** and **FDC-2a** (10.2 and  $9.9 \text{ cm}^3 \text{ g}^{-1}$  at  $P/P_s = 0.98$ , respectively). For zeolite 3A, despite the surface condensation at high  $P/P_s$ , a distinguishable difference between  $\text{H}_2\text{O}$  and  $\text{D}_2\text{O}$  was observed at low  $P/P_s < 0.2$ , which was attributed to the cluster formation of  $\text{H}_2\text{O}$  or  $\text{D}_2\text{O}$  at different  $P/P_s$ . In principle, this difference could be used in discriminating

water isotopologues by controlling the relative pressure. However, in the real recognition/separation systems, an ambient pressure ( $P/P_s$  around 1) is more favorable, whereas low pressure is difficult to control. For  $\text{Ni}_2(\text{bipy})_3(\text{NO}_3)_4\text{-M}$  and  $\text{Ni}_2(\text{bipy})_3(\text{NO}_3)_4\text{-E}$ , they underwent a sudden gate open and a gradual gate open toward  $\text{H}_2\text{O}$  and  $\text{D}_2\text{O}$  molecules in the adsorption process, and therefore, they could not separate water isotopologues. For HKUST-1, it represents the systems using large pores and strong binding sites for the separation of water isotopologues (thus thermodynamic separation). However, no difference could be observed in the sorption curves. Therefore, the demonstrated preferential adsorption of  $\text{H}_2\text{O}$  over  $\text{D}_2\text{O}$  by **FDC-1a** and **FDC-2a** at 298 K was not found for other small-pore adsorbents, including zeolite, activated carbon, and other PCPs/MOFs. Even though some compounds show a slight difference in preference of adsorption behavior for water isotopologues, the difference is not comparable to adsorption behavior by **FDC-1a** and **FDC-2a**.



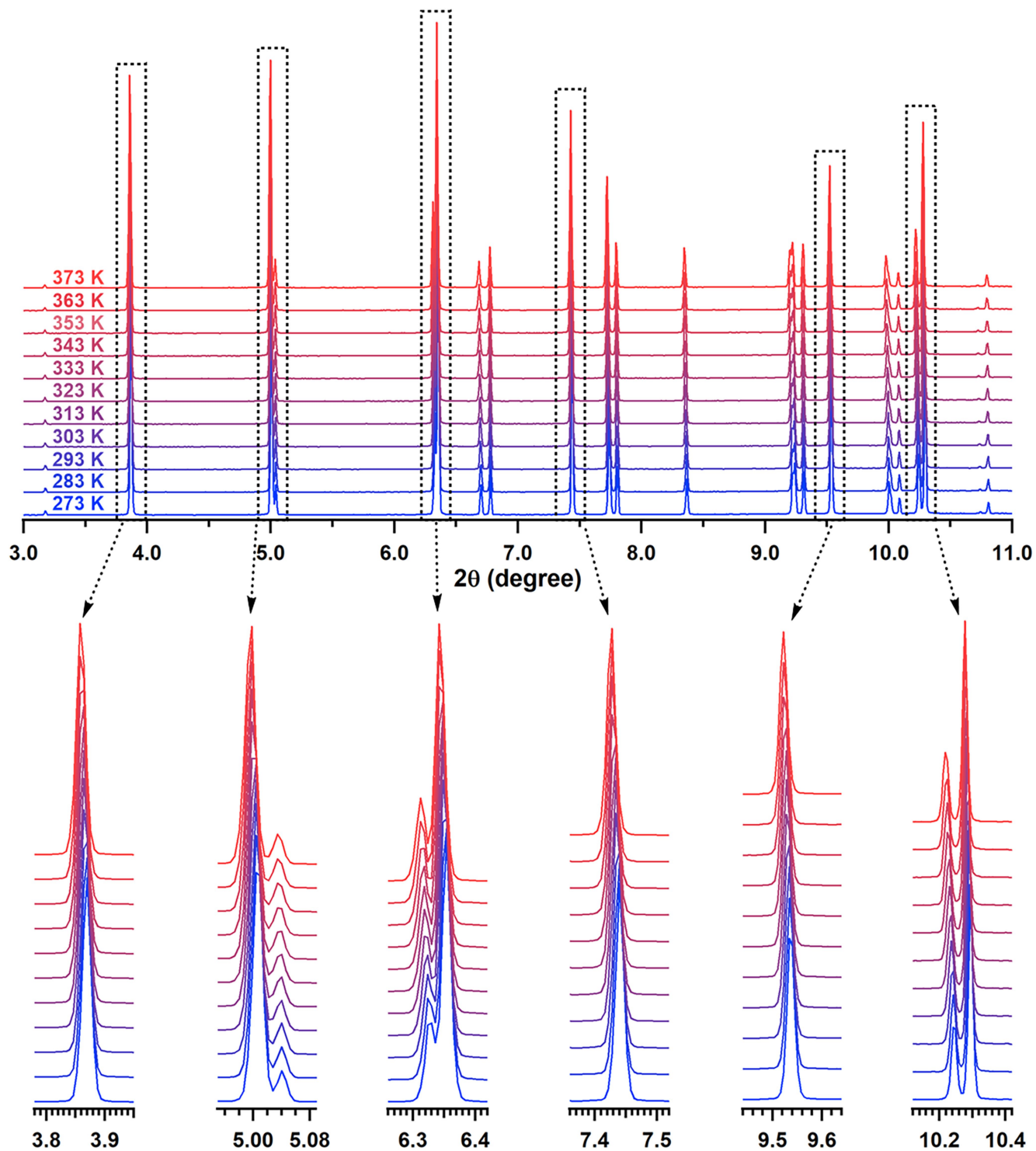
**Extended Data Fig. 2 |  $\text{H}_2\text{O}$  and  $\text{D}_2\text{O}$  sorption curves for FDC-1a and FDC-2a at 298 K using different exposure time.** **a.**  $\text{H}_2\text{O}$  sorption curves for FDC-1a. **b.**  $\text{D}_2\text{O}$  sorption curves for FDC-1a. **c.**  $\text{H}_2\text{O}$  sorption curves for FDC-2a. **d.**  $\text{D}_2\text{O}$  sorption curves for FDC-2a. We measured the  $\text{H}_2\text{O}$  and  $\text{D}_2\text{O}$  sorption curves with the exposure time of each plot as 600 s, 1800 s, and 4800 s, respectively,

resulting in a total measurement time of 26.4, 74.2, and 221.5 h, respectively. The adsorption amounts markedly increased with the prolonged exposure time, which indicated that the diffusion kinetics of adsorbates was the determining factor for this thermoresponsive adsorption behavior.

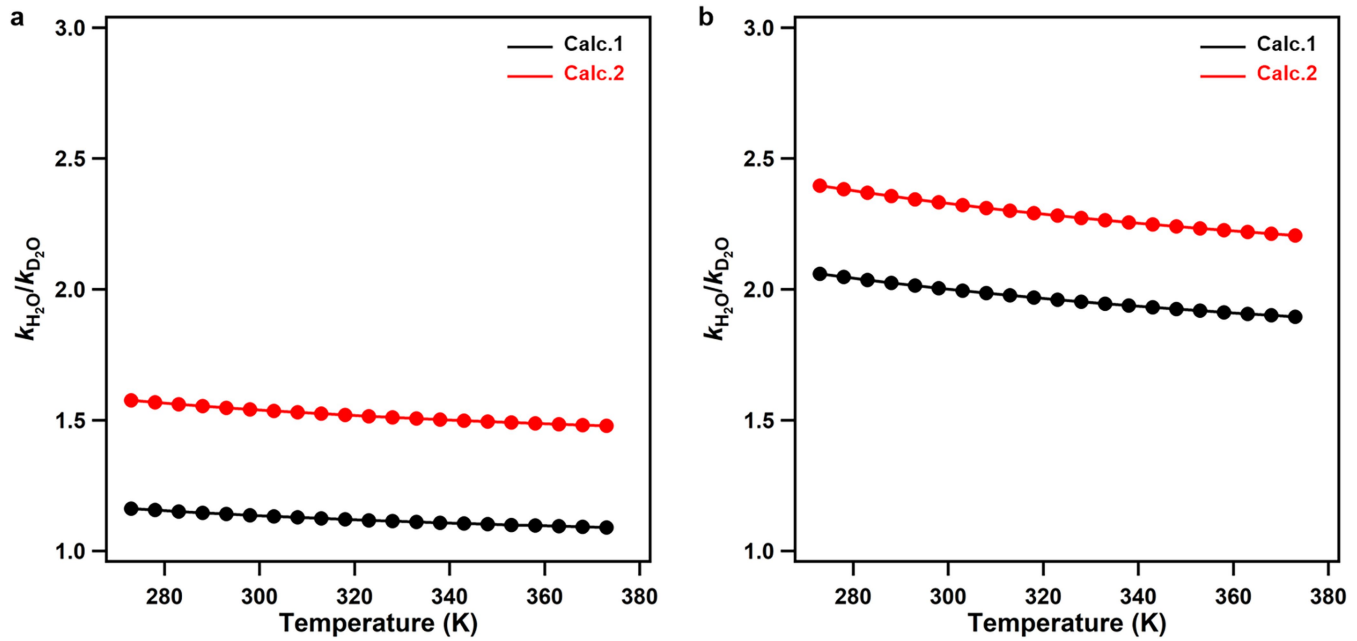


**Extended Data Fig. 3 | Temperature-dependent sorption curves of  $\text{H}_2\text{O}$  and  $\text{D}_2\text{O}$ .** **a**,  $\text{H}_2\text{O}$  sorption curves in **FDC-1a** from 278 to 323 K. **b**,  $\text{D}_2\text{O}$  sorption curves in **FDC-1a** from 278 to 323 K. **c**,  $\text{H}_2\text{O}$  sorption curves in **FDC-2a** from 278 to 323 K. **d**,  $\text{D}_2\text{O}$  sorption curves in **FDC-2a** from 278 to 323 K. The uptake amounts of  $\text{H}_2\text{O}$  and  $\text{D}_2\text{O}$  in both the two PCPs obviously increased as increasing the temperature, indicating a diffusion-controlled sorption behavior which was determined by the kinetic factor. On the other hand, the uptake amounts of  $\text{H}_2\text{O}$

in both the two PCPs were substantially higher than that of  $\text{D}_2\text{O}$  at the same temperature (e.g.,  $\text{H}_2\text{O}$  36.1  $\text{mL g}^{-1}$  vs.  $\text{D}_2\text{O}$  25.9  $\text{mL g}^{-1}$  in **FDC-1a** at 298 K, and  $\text{H}_2\text{O}$  25.2  $\text{mL g}^{-1}$  vs.  $\text{D}_2\text{O}$  15.4  $\text{mL g}^{-1}$  in **FDC-2a** at 298 K), revealing that the diffusion of  $\text{H}_2\text{O}$  was faster than that of  $\text{D}_2\text{O}$ . Finally, under otherwise identical conditions (same temperature and vapor), the uptake amounts of  $\text{H}_2\text{O}$  and  $\text{D}_2\text{O}$  in **FDC-1a** were substantially higher than that in **FDC-2a**, demonstrating that the diffusion rate of the former was higher than the latter.



**Extended Data Fig. 4 | Variable-temperature synchrotron PXRD of FDC-1a under vacuum conditions.** The curves from blue to red denote the temperature changing from 273 to 373 K. The ranges of dominant peaks are enlarged to clearly show the slight change of peak position with temperature.



**Extended Data Fig. 5 | Diffusion-rate calculation.** Diffusion rates ( $k$ ) of  $\text{H}_2\text{O}$  and  $\text{D}_2\text{O}$  in (a) FDC-1a and (b) FDC-2a. Calc.1 represents the calculated diffusion rates considering that all rotational and translational movements were changed to vibrational modes for the adsorbed  $\text{H}_2\text{O}$  or  $\text{D}_2\text{O}$ .

Calc.2 represents the calculated diffusion rates by considering that one rotational movement remains and other rotational and translational movements of  $\text{H}_2\text{O}$  or  $\text{D}_2\text{O}$  were changed to vibrational modes at the initial state.

## Article

**Extended Data Table 1 | Current methods of the separation of deuterated species**

method	working substances	separation factor	working temperature	produced substance	application type	ref
distillation	H <sub>2</sub> /D <sub>2</sub>	1.81	17 K	D <sub>2</sub>	industry	3
gas adsorption	H <sub>2</sub> /D <sub>2</sub>	1.8–9.8	20–30 K	D <sub>2</sub>	lab	25,26
distillation	H <sub>2</sub> O/HDO/D <sub>2</sub> O	1.02	373 K	D <sub>2</sub> O	industry	3
electrolysis	H <sub>2</sub> O/HDO/D <sub>2</sub> O	1.05–2.0	298 K	D <sub>2</sub> O	industry	3
Geib–Spevack process	H <sub>2</sub> O	1.2–2.0	363–473 K	HDO	industry	3
vapor adsorption	H <sub>2</sub> O/HDO/D <sub>2</sub> O	4.4–212.1	298 K	H <sub>2</sub> O	lab	This work

Distillation and gas adsorption for separating hydrogen isotopes; distillation, electrolysis, Geib–Spevack process, and vapour adsorption (this work) for separating water isotopologues.